

**MELT CONVECTION IN WELDING AND CRYSTAL
GROWTH**

by

Minh Do-Quang

December 2004
Technical Reports from
Royal Institute of Technology
Department of Mechanics
SE-100 44 Stockholm, Sweden

Typsatt i $\mathcal{A}\mathcal{M}\mathcal{S}$ - $\mathcal{L}\mathcal{A}\mathcal{T}\mathcal{E}\mathcal{X}$.

Akademisk avhandling som med tillstånd av Kungliga Tekniska Högskolan i Stockholm framlägges till offentlig granskning för avläggande av teknologie doktorsexamen Onsdagen 15 december 2004 kl. 10.15 i Kollegiesalen, Administrationsbyggnaden, Kungliga Tekniska Högskolan, Valhallavägen 79, Stockholm.

© Minh Do-Quang 2004

Universitetservice US AB, Stockholm 2004

MELT CONVECTION IN WELDING AND CRYSTAL GROWTH

Minh Do-Quang 2004

Department of Mechanics,
Royal Institute of Technology
SE-100 44 Stockholm, Sweden.

Abstract

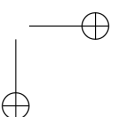
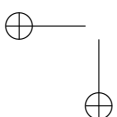
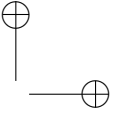
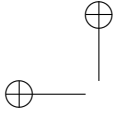
A parallel finite element code with adaptive meshing was developed and used to study three dimensional, time-dependent fluid flows caused by thermocapillary convection as well as temperature and dopant distribution in fusion welding and floating zone crystal growth.

A comprehensive numerical model of the three dimensional time-dependent fluid flows in a weld pool had been developed. This model considered most of the physical mechanisms involved in gas tungsten arc welding. The model helped obtaining the actual chaotic time-dependent melt flow. It was found that the fluid flow in the weld pool was highly complex and influenced the weld pool's depth and width. The physicochemical model had also been studied and applied numerically in order to simulate the surfactant adsorption onto the surface effect to the surface tension of the metal liquid in a weld pool.

Another model, a three dimensional time-dependent, with adaptive mesh refinement and coarsening was applied for simulating the effect of weak flow on the radial segregation in floating zone crystal growth. The phase change equation was also included in this model in order to simulate the real interface shape of floating zone.

In the new parallel code, a scheme that keeps the level of node and face instead of the complete history of refinements was utilized to facilitate derefinement. The information was now local and the exchange of information between each and every processor during the derefinement process was minimized. This scheme helped to improve the efficiency of the parallel adaptive solver.

Descriptors: thermocapillary convection, gas-tungsten arc welding, floating zone, parallel computing, finite element method, automated code generation.



Preface

This thesis considers the study of thermocapillary convection in fusion welding and floating zones and the role of surfactant redistribution in welding. The thesis is based on and contains the following papers.

Paper 1. DO-QUANG, M. AND AMBERG, G. 2003 'Modelling of Time-Dependent 3D Weld Pool Flow Due to a Moving Arc'. *Proceedings of High Performance Scientific Computing*. March 2003, Hanoi-Vietnam.

Paper 2. DO-QUANG, M. AND AMBERG, G. 2003 'Modelling of Time-Dependent 3D weld pool flow'. Accepted for publication in *Mathematical modelling of weld Phenomena 7*.

Paper 3. DO-QUANG, M., AMBERG, G., AND PETTERSSON, C. 2004 'Experimental and Numerical study of the influence of sulfur redistribution in welding of SAF-2507 stainless steel'. Submitted to *Science & Technology of Welding & Joining*

Paper 4. DO-QUANG, M., AMBERG, G., AND PETTERSSON, C. 2004 'Modelling of the adsorption kinetics and the convection of surfactants in GTA welding'. *To be submitted*.

Paper 5. DO-QUANG, M., AMBERG, G., AND CARLBERG, T. 2004 'Three-dimensional time dependent modelling of radial segregation due to weak convection'. *Journal of crystal growth*, **269**, p.454,

Paper 6. DO-QUANG, M., SINGER-LOGINOVA, I. VILLANUEVA, W. AND AMBERG, G. 2004 'Problem Solving Environment for Parallel Adaptive Computation'. Submitted to *Mathematics and Computers in Simulation*.

The papers are re-set in the present thesis format.

Division of work between authors

Paper 1. The author of the thesis has developed the parallel code as well as implemented the weld problem, made the simulation and wrote this paper with guidance of Gustav Amberg.

Paper 2. The respondent made the simulations and wrote the report with supervision of Gustav Amberg. The experimental work on the 645 SMO steel was carried out at AvestaPolarit Stainless AB.

Paper 3. This paper is the result of collaboration research with Sandvik Stainless AB. The experiment was conducted by Claes-Ove Pettersson. The respondent performed the numerical parts and documented the paper with guidance and correction of Gustav Amberg.

Paper 4. The author made the simulations and write the paper with supervision of Gustav Amberg. The author made the experimental studies with helped from Claes-Ove Pettersson.

Paper 5. The experimental work had been carried out at the Mid Sweden University in Sundsvall, Sweden by the co-author, T. Carlberg. The mathematical implementation and simulations were done by the author of the thesis.

Paper 6. The respondent developed the code, verified the scheme and wrote the report for the welding simulation part. Walter Villanueva was responsible for the literature reviews and documentation of this paper with guidance of the author of this thesis. Irina Singer-Loginova made the phase-field simulations and Walter Villanueva made the simulations of wetting phenomena.

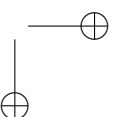
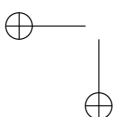
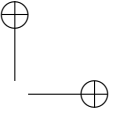
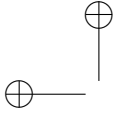
Contents

Preface	v
Chapter 1. Introduction	1
Chapter 2. Materials processes	5
2.1. Gas tungsten-arc welding	5
2.1.1. Introduction	5
2.1.2. Mathematical modelling	8
2.2. Floating zone method	11
2.2.1. Introduction	11
2.2.2. Mathematical modelling	14
Chapter 3. Modelling surfactant mass transfer in liquid metal system	17
3.1. Overview	17
3.2. Numerical model	19
Chapter 4. Numerical methods	21
4.1. Solving algorithm	21
4.2. Parallel adaptive computation	22
4.3. Automated code generation	25
Chapter 5. Summary of papers	27
Chapter 6. Conclusions and outlook	29
Acknowledgment	31
Bibliography	33
Part 1. Papers	37
Modelling of Time-dependent 3D Weld Pool	41
1. Introduction	41

viii CONTENTS

2. Physical phenomena	42
3. Modelling approach	43
3.1. Mathematical Modelling	43
3.2. Numerical Modelling	45
4. Results and Discussion	46
4.1. 3D simulation of the welding pool with a stationary arc	46
4.2. Effect of moving heat source speed	48
4.3. Time dependent	49
5. Conclusions	51
References	51
Modelling of time-dependent 3D weld pool flow	55
1. Introduction	55
2. Physical phenomena	56
3. Modelling approach	57
3.1. Mathematical formulation	57
3.2. Numerical Modelling	60
4. Results and discussion	61
4.1. AP5 (high sulfur content):	61
4.2. AP1 (low sulfur content)	66
4.3. 654-SMO (extra low sulfur content)	69
5. Conclusions	72
References	73
Experimental and Numerical study of the influence of sulfur redistribution in welding of SAF-2507 stainless steel	79
1. Introduction	79
2. The marangoni effect in welding	80
3. Mathematical modeling	81
3.1. Surfactant transport equations	83
3.2. Langmuir adsorption isotherm	83
4. Experimental study	85
5. Results and discussion	86
5.1. Case 1: $I = 100A, U_s = 200 \text{ mm min}^{-1}$	87
5.2. Case 2: $I = 200A, U_s = 200 \text{ mm min}^{-1}$	90
5.3. Case 3: $I = 200A, U_s = 100 \text{ mm min}^{-1}$	96
6. Conclusions	100
References	100

Modeling of the adsorption kinetics and the convection of surfactants in GTA welding	105
1. Introduction	105
2. Mathematical modeling	106
2.1. Surfactant mass transfer	107
2.2. Thermodynamics of adsorption	109
2.3. Numerical modelling	110
3. Results and discussion	112
4. Conclusions	118
References	120
Three-dimensional time dependent modelling of radial segregation due to weak convection	125
1. Introduction	125
2. Experimental results	126
3. Mathematical Modelling	128
3.1. Governing equations	128
3.2. Boundary conditions	130
3.3. Numerical method	131
4. Results and discussion	132
5. Conclusions	137
References	138
Problem Solving Environment for Parallel Adaptive Computation	141
1. Introduction	141
2. Implementation	143
3. Applications	147
3.1. Welding	147
3.2. Free Boundary Problem	150
3.3. Dendritic solidification	152
4. Conclusion	153
Appendix	154
References	158



CHAPTER 1

Introduction

Recently, the importance of material processes has been growing rapidly and are continuing to increase. Joining processes and crystal growth, for example, which involve complex phenomena at high temperature and with moving interfaces, have been widely applied in many industries. Being able to understand these phenomena, we can assist in the process optimization.

Joining processes have a very long history. From the Bronze Age, small gold circular boxes were made by pressure welding lap joints together. In the early Iron Age, Blacksmith practised the art of shaping heated iron and steel (forging) with hand tools such as hammers.

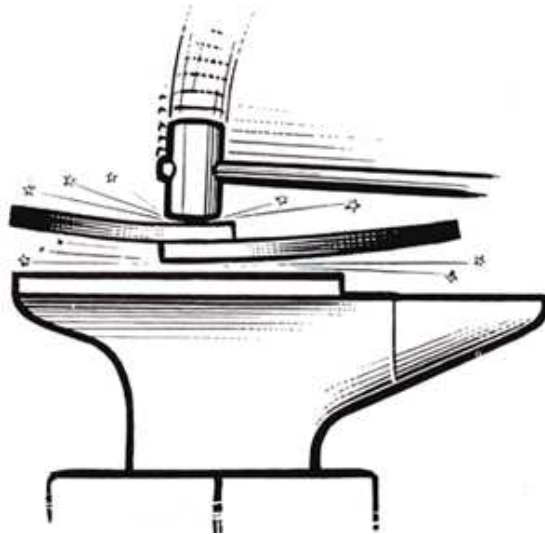


FIGURE 1.1. The forge weld

The Blacksmith’s forge weld involved both heat and pressure. In this method, fusion weld was not entailed. However, the material is heated to the plastic range. Under the influence of applied pressure (hammering), the hot working of the metal parts ensured an intimate bond with a re-crystallization into one homogeneous mass, Figure 1.1. The forge method was still a purely solid-phase process and gradually disappeared after the solid-liquid-phase joining method was introduced by Edmund Davy

2 1. INTRODUCTION

in 1836. It became predominant and wide-spread from the First World War. This kind of joining is characterized as a highly complex technical process and has been broadly applied in various applications, from ship building industry to semiconductor production. The complexity of the method has been well recognized, especially when there is more than one material to appear in different phases (i.e. solid, liquid or gaseous phase) at the same time. In addition, many other different physical phenomena could involve in the joining process.

A similar problem also occurs in the field of semiconductor crystal growth, which attracted enormous interest over the last decades. Single crystals of silicon, for example, represent the bedrock upon which all modern electronics is built, from telecommunications to consumer electronics, from gaming consoles to life-saving medical equipments. Unsurprisingly, silicon wafers did not simply grow on trees. They first have to be produced as an extremely pure chemical and then grown as single crystals under very specific conditions. The first synthetic gem stones were made in the mid-1800s, and methods for making high-quality crystals of various materials have been developed over the course of the past century.

One of the methods to achieve this high quality is the floating zone method. The main difference of the floating zone method compared to the others is the fact that any contamination from a crucible material is avoided. This is achieved by using a freestanding rod of polycrystalline, e.g. silicon, fixed at one end with a pull rod.

Fundamental mechanisms of the two above material processes are certainly well documented. Most of researches on these phenomena mainly focus on the analysis of the respective process using experimental techniques. However, as the characteristic of the two material processes mentioned above, the temperature in the weld pool or in the liquid bridge usually reaches the higher temperature than the melting temperature. Therefore, it is almost impossible to identify the physical and chemical processes inside a liquid pool by experimental methods. Meanwhile, in order to understand the development of the weld from the early stage as well as the influence of the input conditions to the different weld pool shapes, an inclusive study of the fluid flow in the respective liquid zones is required.

Numerical analysis recently has developed and becomes more useful for fundamental study of material processes. Although natural phenomena in material processes are very complicated and difficult to describe in terms of applied mathematics, numerical modelling in combination with corresponding experimental studies is certainly the most powerful tool to conduct the research described above.

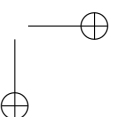
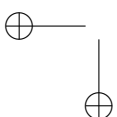
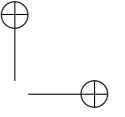
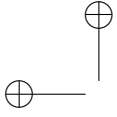
In this thesis, the following aims had been targeted:

1. To apply and develop a powerful tool of automated code generation for numerical modelling of physical phenomena, which occurred in the two material processes of fusion welding and the floating zone;
2. To expand the 2D model from previous work to a 3D model in order to study the unstable, asymmetric flows in a real case.

A good agreement could be obtained when the computed results are compared to the corresponding experimental outputs. The results also help to reveal shortcomings

1. INTRODUCTION 3

of new mathematical models. The work is therefore organized as a cooperation between fluid mechanics and material science. Here, thermo-capillary convection is the main driving force of fluid flow in both fusion welding and floating zone, and is thus importance for these material processes.



CHAPTER 2

Materials processes

2.1. Gas tungsten-arc welding

2.1.1. INTRODUCTION

The primary goal of any welding operation is to make a weld having the same properties as the base metal. The only way to produce such a weld is to protect the molten puddle from the atmosphere. In gas shielded-arc welding, an inert gas is used as a covering shield around the arc to prevent the atmosphere from contaminating the weld. Gas shielding makes it possible to weld metals that are otherwise impractical or difficult to weld by eliminating atmospheric contamination of the molten puddle.

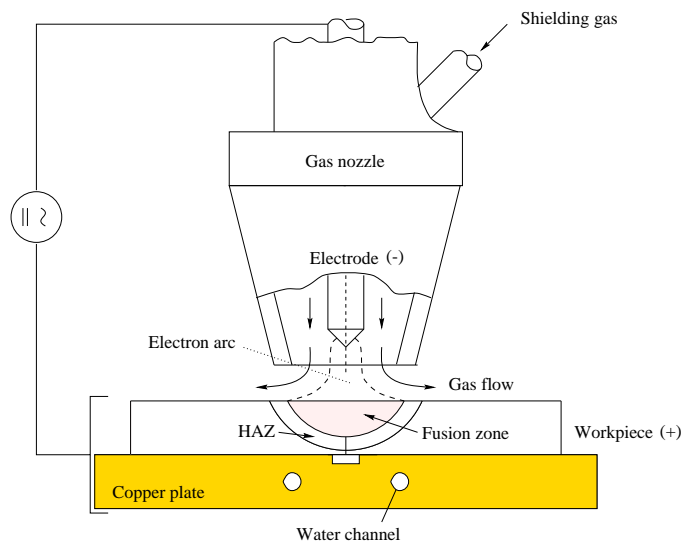


FIGURE 2.1. Principle of the GTAW technique

Gas tungsten-arc welding (GTA) is a form of shielded-arc welding. However, in gas tungsten-arc welding, the electrode is used only for creating the arc. The electrode is not consumed in the weld as in the shielded metal-arc process. As shown in Figure 2.1, the basic GTA process involves an intense arc between the base metal and a tungsten electrode. The arc, the electrode, and the weld zone are surrounded by an inert gas (i.e. either helium or argon or a mixture of the two as usual) that displaces

6 2. MATERIALS PROCESSES

the air and eliminates the possibility of weld contamination by the oxygen and nitrogen present in the atmosphere. The high melting point of tungsten electrode made it virtually non-consumable.

Nowadays, GTA welding has become an indispensable tool for many industries since high-quality welds are produced with low equipment costs. The process uses shielding gas without the application of pressure. The process might be used with or without the addition of filler metal as well. The principle of the GTA welding is shown in Figure 2.1. The electrode, as seen in Figure 2.1, is the cathode and the work-piece is the anode. Primarily electrons obtained by ionization of the inert gas atoms and emitted by the negative electrode, carried the arc current. The electrons are attracted towards the positive work-piece where they generate the necessary heat to melt the work-piece edges of the two materials to be joined. Thus, a weld fusion zone containing liquid material is formed and often denoted as weld pool. An overview of the phenomena driving the weld pool formation and the directions of their actions on the heat and mass transport are schematically shown in Figure 2.2.

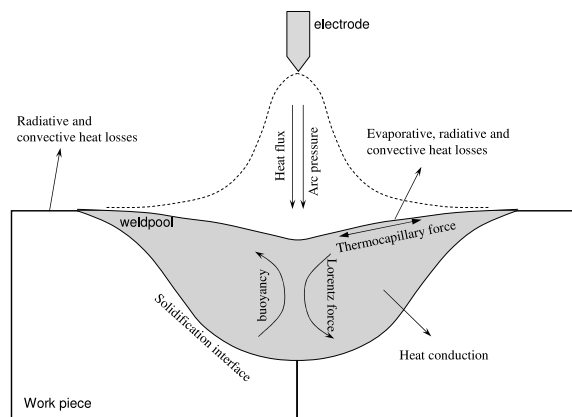


FIGURE 2.2. Physical phenomena driving the heat and fluid flow in the weld pool

From Figure 2.2, it is obvious that the fluid flow in the weld pool is very complex and mainly driven by forces due to surface tension gradient, buoyancy, electromagnetic, arc pressure and aerodynamic drag force arising from the shielding gas used in GTA welding. The shielding gas cools the weld pool surface at the top surface of the work-piece and creates convective cooling at this location. There are also a radiative heat losses, an evaporation of various elements from the weld pool, which decreases the local surface temperature. Therefore, a comprehensive numerical model needs to be studied.

In the last two decades, considerable progress has been made in modelling and numerical simulation of fluid flow and heat transport phenomena in GTA welding. A great number of models have been published in this subject. Atthey (1980) considered

2.1. GAS TUNGSTEN-ARC WELDING 7

the fluid flow in the weld pool driven by electromagnetic forces only, thus neglecting the heat flow. Oreper *et al.* (1983) and Oreper & Szekely (1984) were the first to present a mathematical model describing fluid flow as well as heat flow in a stationary weld pool and considering buoyant, electromagnetic and surface tension forces. The basic assumptions in their modelling is still applied today. Kou & Le (1983) carried out a three-dimensional, theoretical and experimental study on heat flow and solidification during the welding of aluminum plates and concluded that the model would be useful in predicting the weld penetration.

Most of the mathematical models were simplified by assuming that the two metal plates to be joined could be represented as one work-piece and considered stationary welding implying that the electrode was not moving. It was held stationary over the plate to be welded. The simplified mathematical model thus became axisymmetric and could be used to study the development of the weld pool. Zacharia *et al.* (1991); Winkler *et al.* (1998); Ehlen *et al.* (2001).

The physical phenomena in the weld pool are very complex and appear in a high temperature environment. Therefore, it is difficult to get appropriate data for the physical properties such as the thermo-physical properties of materials at high temperatures, especially exceeding the melting point. There has been a lack of knowledge of heat and current fluxes on the weld pool surface as well. It has generally been difficult to obtain a good correspondence between numerical calculation and experimental results in terms of exact weld pool shape, or weld pool surface temperature, or heat balance. The most detailed comparison of predicted and measured GTA weld pool shapes has been presented in works of Zacharia *et al.* (1989*a,b*, 1991) and Winkler *et al.* (1998). They concluded that, with higher amounts of sulfur content than the nominal sulfur content in the stainless steel, the numerical solution of weld pool shape should be deepen and bring in a good agreement with the experiment.

In those works, the fluid flow was considered as a laminar flow, while others considered it as turbulent. Mundra *et al.* (1996, 1997); Choo & Szekely (1992, 1994); Palmer & DebRoy (2000) have employed rudimentary 'zero equation' turbulence models in their models. The turbulent flow in the weld pool has been taken into account by enhancing both viscosity and thermal conductivity.

Recently, Yang & DebRoy (1999); Yang *et al.* (2000); Zhao & DebRoy (2001) and Chakraborty *et al.* (2004) also used the $k - \epsilon$ turbulence model for modelling the fluid flow in the weld pool. Hong *et al.* (2002) developed a sophisticated dynamic mesh re-mapping model in order to resolve the solid-liquid interface region which was important for the wall function.

The model considered heat flux from the arc to the work-piece is very important since it affects the weld pool shape and the distribution of the temperature on the surface of the work-piece. During the late 1930s and in the mid-1940s, Rosenthal (1941, 1946) introduced an analytic treatment of the heat distribution in welding. He used a moving coordinate system and developed a solution for the Fourier partial differential equation (PDE) of heat conduction. To facilitate solution of the PDE, Rosenthal assumed quasi-steady-state conditions that could be justified experimentally. From the pioneering work of Rosenthal, many researchers express the thermal aspects of

8 2. MATERIALS PROCESSES

welding at the surface and between electrode and work-piece. Eager & Tsai (1983) modified Rosenthal’s model by including a two-dimensional Gaussian distributed heat source and developed a solution for traveling heat source on a semi-infinite plate to provide the size and the shape of the arc weld pools. Zacharia & Eraslan (1988*b,a*) developed a transient thermal three-dimensional models for both autogeneous and non-autogeneous welding.

In our related works, cf. papers 1 and 2, the disagreement between experimental and numerical weld pool shapes have been overcome by adapting the surface active element as introduced by Zacharia *et al.* (1991); Winkler *et al.* (1998). Meanwhile, a physicochemical surfactant mass transfer model for binary and multi-component alloys was used on paper 3 and paper 4. Those models considered surfactant mass transfer and will be discussed in the next section. More details are referred to the related papers in this thesis.

2.1.2. MATHEMATICAL MODELLING

This section presents a summary of the mathematical model of the weld pool. The model, which is applied in the papers, will be presented in the papers’ section of this thesis, as well as the sub-models are discussed as they enter the weld pool modelling effort at the boundaries. The melt is treated here as an incompressible Boussinesq liquid in the welding pool.

$$\nabla \cdot \mathbf{u} = 0 \quad (2.1)$$

$$\frac{\partial \mathbf{u}}{\partial t} + (\mathbf{u} \cdot \nabla) \mathbf{u} - \frac{\partial(U_s \mathbf{u})}{\partial y} = -\frac{1}{\rho} \nabla p + \nabla \cdot \mathbf{v} (\nabla \mathbf{u} + \nabla \mathbf{u}^T) + \mathbf{S} \quad (2.2)$$

where, \mathbf{u} is the fluid velocity; p is the pressure, and \mathbf{S} is the source term that includes the Lorentz force, gravity, etc. The thermal energy conservation is expressed as follows:

$$\frac{\partial T}{\partial t} + (\mathbf{u} \cdot \nabla) T - \frac{\partial(U_s T)}{\partial y} = \alpha \Delta T + \frac{L^*}{\rho C_p} \left(\frac{\partial \chi}{\partial t} - \frac{\partial(U_s \chi)}{\partial y} \right) \quad (2.3)$$

where α is the thermal diffusivity, C_p is the specific heat and L^* is the latent heat of fusion. Those physical properties - the thermal diffusivity, the specific heat and the heat conductivity are assumed independent from the temperature in the present work. The two terms containing U_s appears as a result of the coordinate transformation. In this way, the simulation domain is attached to the arc to simplify the moving arc problem. The action of volumetric forces on the melt is described by the source term \mathbf{S} :

$$\mathbf{S} = \frac{1}{\rho} (\mathbf{J} \times \mathbf{B}) + \frac{\mathbf{v}}{H(\chi)} \mathbf{u} + \mathbf{g} \beta (T - T_{ref}) \quad (2.4)$$

The Lorentz force components are included in the source term as a product of $\mathbf{J} \times \mathbf{B}$, in which the solenoidal vectors \mathbf{J} and \mathbf{B} are the current density vector and magnetic flux vector. Those are calculated by solving the Maxwell’s equations of the

2.1. GAS TUNGSTEN-ARC WELDING 9

electromagnetic field in the domain of the work-piece. Assuming the effect of fluid motion on the electromagnetic field is small, the Lorentz forces become constant and are included in the system equations as a known body force. The \mathbf{J} and \mathbf{B} fields are axisymmetric and analytical solution for the Lorentz forces (can be obtained as in Kou & Sun (1985)). Using cylindrical-coordinate system r, z, ϕ , which the z axis as electric arc centre line, \mathbf{J} and \mathbf{B} fields given by,

$$\mathbf{B} = [0, 0, B_\phi] \quad (2.5)$$

$$\mathbf{J} = [J_r, J_z, 0] \quad (2.6)$$

where, different components of the current distribution and the magnetic flux are obtained as

$$J_r = \frac{I}{2\pi} \int_0^\infty \xi I_1(\xi r) e^{-z\xi} e^{-\frac{\xi^2 b^2}{12}} d\xi \quad (2.7)$$

$$J_z = \frac{I}{2\pi} \int_0^\infty \xi I_0(\xi r) e^{-z\xi} e^{-\frac{\xi^2 b^2}{12}} d\xi \quad (2.8)$$

$$B_\phi = \frac{\mu_m I}{2\pi} \int_0^\infty I_1(\xi r) e^{-z\xi} e^{-\frac{\xi^2 b^2}{12}} d\xi. \quad (2.9)$$

J_r and J_z are the r-component and the z-component of the current distribution and B_ϕ is the azimuthal-component of the magnetic flux vector. I_0 and I_1 are the Bessel functions of the first kind and of order zero and one. The Lorentz forces in the cylindrical-coordinate system now can be converted to the Cartesian coordinate system as,

$$(\mathbf{B} \times \mathbf{J})_x = J_r B_\phi \cos \phi \quad (2.10)$$

$$(\mathbf{B} \times \mathbf{J})_y = J_r B_\phi \sin \phi \quad (2.11)$$

$$(\mathbf{B} \times \mathbf{J})_z = J_z B_\phi \quad (2.12)$$

The second source term in equation (2.4) originates from the consideration that the morphology of the phase-change domain could be treated as an equivalent porous medium at the solid-liquid interface. Thus, it helped to avoid the interface tracking problems since the interface came out from the solution procedure itself. Here χ is the fraction of volume occupied by melt, χ has a value of 0 in the solid region, and 1 in the completely molten region. $H(\chi)$ is the permeability of the mush, Amberg (1991). $H(\chi)$ is infinite in the molten region and very rapidly decreases to very small values (i.e. 10^{-8}) in the solid region. Therefore, the velocity \mathbf{u} becomes effectively zero in the solid region. Neglecting the presence of a mushy-zone by assuming the material changes directly from solid to liquid, the fraction of volume occupied by that solid can be computed according to Amberg (1991),

$$\frac{\partial \chi}{\partial t} = \frac{1}{\kappa} (T - T_{liq}) \quad (2.13)$$

10 2. MATERIALS PROCESSES

In this equation, κ is a purely numerical parameter and T_{liq} is the liquidus temperature. This equation is a simple way to determinate of the solid fraction χ at the new time level by using the discretized form of the left-hand side: If χ tends to exceed 1 or decrease below 0, the new value of χ is taken to be 1 or 0, respectively. This means that, T then allowed to differ from the non-dimensionless of the melting temperature T_{liq} , which is, obviously, quite correct in the solid ($\chi = 0$) or the liquid ($\chi = 1$) region. The numerical parameter κ is a small constant, used for amplifying any deviation of the temperature from T_{liq} , resulting in a rapid melting or freezing that restores T to T_{liq} .

Boundary conditions:

It is very well established that the heat input from the arc could be simulated using a Gaussian distribution as, Eager & Tsai (1983); Zacharia & Eraslan (1988b,a),

$$q_{gauss} = \frac{3Q}{\pi r_a^2} \exp\left(-\frac{3(x^2 + y^2)}{r_a^2}\right) \quad (2.14)$$

where $Q = EI\eta$ is the total heat input, E is the arc voltage, I is the electric current, r_a is the effective radius of heat distribution and defined as the distance where the heat flux decay to 5% of its maximum value. The arc efficiency η usually depend on the rate of heat transfer from electrode to the work-piece and is very difficult to obtain theoretically. Here η varied from 20 to 95%, cf. Kou (2002).

The evaporation of liquid metal in the weld pool was considered, since the weld pool surface temperatures could be greater than the melting temperature. Khan & DebRoy (1984) claimed that the inclusion of vapor composition in the model helped to lower the maximum temperature in the weld pool. Here, the evaporation heat flux is computed according to Kim (1975).

$$q_{evap} = W \cdot h_{fg} \quad (2.15)$$

where q_{evap} denotes the evaporation heat flux and h_{fg} is the heat of evaporation. W is obtained by using an equation

$$W = \exp(A_1 + \log(p_{atm}) - 0.5 \cdot \log(T)) \quad (2.16)$$

where A_1 is a constant varying slightly for the different species of the material to be treated and p_{atm} is the vapor pressure as obtained from Kim (1975)

$$\log(p_{atm}) = 6.121 - \frac{18.836}{T} \quad (2.17)$$

The radiative q_{rad} and convective q_{conv} heat losses could be calculated using

$$q_{rad} = \sigma_b \varepsilon (T^4 - T_a^4) \quad (2.18)$$

and

$$q_{conv} = h_c (T - T_a) \quad (2.19)$$

where σ_b is the Stefan-Boltzmann constant, ϵ the emissivity of steel, h_c the convection heat transfer coefficient, expressing the convective heat exchange between the melt surface and the environment, and T_a is the ambient temperature. The complete thermal boundary condition then becomes

$$-k \frac{\partial T}{\partial z} = -q_{gauss} + q_{evap} + q_{rad} + q_{conv} \quad (2.20)$$

where, k is the thermal conductivity.

At the top surface of the weld pool, the surface tension gradient also enters as a boundary condition for shear stress on the free surface (index s indicate a surface gradient operator):

$$\mu \left((\nabla \mathbf{u}) + (\nabla \mathbf{u})^T \right) \cdot \mathbf{n} = \nabla_s \gamma = \frac{\partial \gamma}{\partial T} \cdot \nabla_s T \quad (2.21)$$

Here, the temperature coefficient of surface tension $\frac{\partial \gamma}{\partial T}$ will be computed in conformity with the Gibbs and Langmuir adsorption isotherms theory. This will be presented below.

2.2. Floating zone method

2.2.1. INTRODUCTION

There are a number of industrial processes for producing single crystals. So far, the most popular process is the crystallization from the melt (i.e. growing a solid crystal from the liquid). The techniques of melt growth can be subdivided into three types: pulling from melt, directional solidification in a crucible and crucible-free methods. The simplest method is the pulling from melt, which was first applied in 1948 at Bell Laboratories of USA. The pulling from melt technique is named after Jan Czochralski, who published the principle in 1917. In the Czochralski method, the molten material is kept in a rotating crucible with a free surface at the top, and the grown single crystal is extracted from the liquid surface in the container. By using the container to grow a single crystal, probability of impurities in the crystal is increased and the purity of the semiconductor crystal could be reduced. However, in the floating zone method, another pulling from melt method hasn't got any contamination from the crucible material. This was achieved by using a freestanding rod of polycrystalline material, for example silicon, fixed at one end with a pull rod.

Figure 2.3 shows a schematic drawing of the floating zone process that was first introduced by Pfann (1952) and used for the preparation of semiconductor grade germanium from 1955. Since that time, the method has been successfully applied to other semiconductors and metals. In this method, only a part of the material is melted at time and a relatively narrow molten zone is passed through a relatively long solid material (feed rod). The single crystal grows from an originally polycrystalline feed rod at the narrow melted zone between two rods, one single crystal and one polycrystalline. The heat source here is usually induction, radio frequency induction, electron beam or laser heating. The molten zone takes the form of a liquid drop place in between the two rods. Obviously, the molten zone is kept in place by surface tension

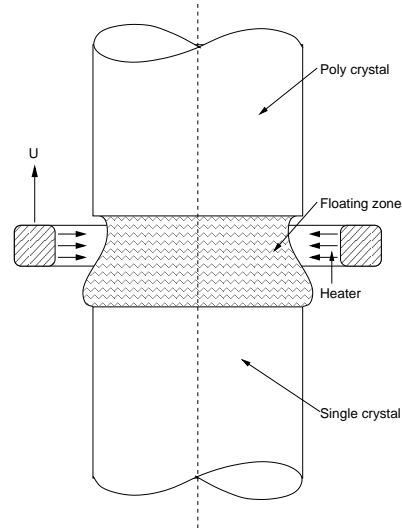


FIGURE 2.3. Principle of the floating zone technique with a radial frequency heat source

forces, which had to be sufficiently strong to balance the static pressure presented at terrestrial conditions. This balance does not function for all semiconductor materials, and limits the use of this method in a gravitational field. Therefore, the floating zone method has been used experimentally in space where micro-gravity conditions are applicable. By avoiding the use of a container, this method is suitable to grow very pure single crystal semiconductor materials.

The convection in the melt zone is mainly driven by the physical mechanisms: buoyancy-driven convection, forced convection from the artificial sources and Marangoni convection. It has a strong impact on the transport of heat, which controls important features in melt growth, such as the shape of the solid-liquid interface and thermal stresses in the growing crystal. The convective transport also determines the distribution of solute in the melt, especially rejecting species in front of the growth interface. Hence, it determines the composition of the crystal on both macro- and micro-scale.

The flows in the Czochralski crucible are the most complicated flows. Typically, the flows, which are time dependent and close to turbulent state, cause strong temperature fluctuations in front of the solidification interface. That leads to compositional fluctuations of the growth crystal and causes micro-segregation. Macro segregation, on the other hand, promotes a steady flow. Therefore, the macro-segregation often occurs in micro-gravity environment experiments, when the non-stationary convection is absent.

The segregation of solutes at the melt-crystal interface leads to the non-uniformity of constituents and impurities in crystals grown from the melt. In equilibrium, which is established when gradients in concentration and temperature are small, the solute concentration C_S in the solid phase relates to the solute concentration C_L in the melt

according to the phase diagram as shown in Fig. 2.4. When the solute concentration is very low, as in the case of semiconductor dopant, an approximate relation can be used as $k = C_S C_L^{-1}$, where k is the equilibrium partition coefficient.

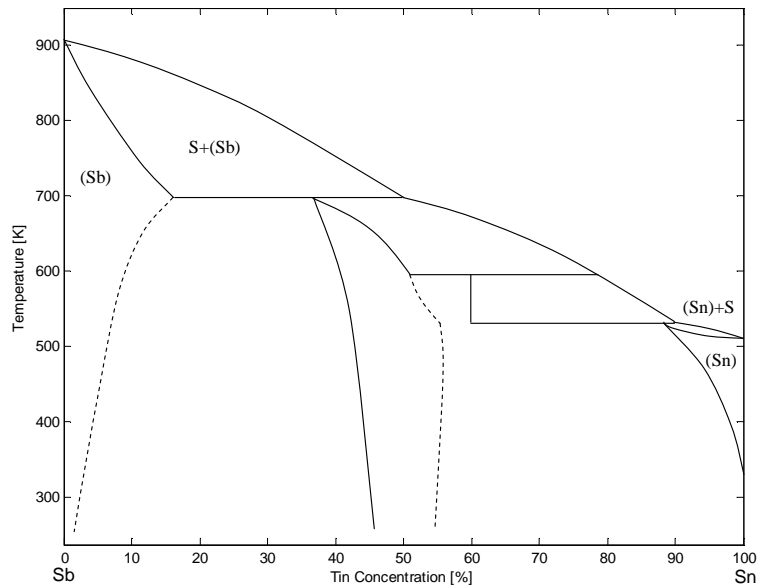


FIGURE 2.4. The phase diagram of Sb-Sn alloy, Jönsson & Ågren (1986)

During actual cooling stage with small cooling rate, the solute is rejected (for $k < 1$) or preferentially absorbed (for $k > 1$) by the advancing solid-liquid interface, forming an enriched or depleted solute layer in front of it. At the low freezing rates used in crystal growth, the solute concentration in the growing crystal may related to the melt concentration at the interface $C_L(0)$, by the relation $C_S = kC_L(0)$, Müller (1998), where k still is the equilibrium segregation coefficient. Meanwhile, $C_L(0)$ depends on the melt convection, which controls the transport of solute atoms in the melt. Taking advantage of the relation between the melt concentration at the interface and the solute concentration in the growing crystal, some works (Levenstam *et al.* (1990); Winkler *et al.* (2000a)) simplified the calculations and assumed that the solidification interface was flat and used that for one of the boundary conditions. This became a simpler problem, when we did not have to compute the shape of the solidifying front.

The growth process of silicon crystals grown with the floating zone method is strongly influenced by convection in the melt zone. Several theoretical studies have indicated that weak convection, with flow rates of the same order of magnitude as the growth rate, can give strong radial segregation Nikitin *et al.* (1981); Chang & Brown (1983); Alexander *et al.* (1989); Polezhayev & Nikitin (1989). Recently, Carlberg (2004) studied the weak convection in a space environment experiment, in which

thermo-capillary forces was used to control the weak flows through a partially coated geometry.

Most of the numerical models for floating zone crystal growth were two dimensional, Lie & Walker (1990); Lan (1996); Mühlbauer *et al.* (1995, 1999), in which the heat and mass transfer, fluid flow and the zone shape were taken into account. In fact, the fluid flow in the molten zone is an unsteady 3D flow. There are several 3D simulations reported by Levenstam *et al.* (1990); Winkler *et al.* (2000a). Those models used a simplified flat interface for the molten zone. Ratnieks *et al.* (2001) modeled the needle-eye floating zone where the shape of the interface was computed from a 2D steady-state model. Recently, Lan & Yeh (2004) reported the steady-state results for a zone shape obtained from an almost steady state solution.

2.2.2. MATHEMATICAL MODELLING

In this section the numerical model used for crystal growth in this thesis will be overviewed. The three dimensional time-dependent model included a phase equation to simulate the real interface shape for the floating zone in a space environment. In space, the coupling between the energy equation and the momentum equations could only occur via the boundary conditions at the free surface. The melt was treated as an incompressible Newtonian liquid and governed by the incompressible Navier-Stokes equations, continuity equation and energy equation as

$$\frac{\partial \mathbf{u}}{\partial t} + (\mathbf{u} \cdot \nabla) \mathbf{u} = -\nabla p + \frac{1}{Re} \nabla \cdot (\nabla \mathbf{u} + \nabla \mathbf{u}^T) + \frac{1}{H(\chi) Re} \mathbf{u} \quad (2.22)$$

$$\nabla \cdot \mathbf{u} = 0 \quad (2.23)$$

$$\frac{\partial \theta}{\partial t} + (\mathbf{u} \cdot \nabla) \theta = \frac{1}{RePr} (\nabla^2 \theta) + \frac{1}{Ste} \frac{\partial \chi}{\partial t} \quad (2.24)$$

where, \mathbf{u} is the fluid velocity; p is the pressure and θ is the temperature. The extra term in the Navier-Stokes equation, Eq. (2.22), represents the porous medium model at the solid-liquid interface. χ is the fraction of volume occupied by melt, χ has a value of 0 in the solid region, 1 was the completely molten region. $H(\chi)$ is the permeability of the mush Amberg (1991). $H(\chi)$ is infinite in the molten region and very rapidly decreases to very small values (i.e. 10^{-8}) in the solid region. Therefore, the velocity \mathbf{u} becomes effectively zero in the solid region. According to Amberg (1991), the fraction of volume occupied by solid can be computed as following:

$$\frac{\partial \chi}{\partial t} = \kappa (\theta - \theta_{liq}) \quad (2.25)$$

where κ is a small numerical parameter, which amplify the temperature difference $(\theta - \theta_{liq})$ and enter to the energy equation as a high value of $\partial \chi / \partial t$. This causes a rapid return to the liquid temperature θ_{liq} from T as melting of freezing occurs. It is referred to equation (2.13) for more details .

2.2. FLOATING ZONE METHOD 15

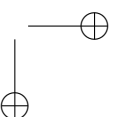
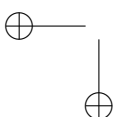
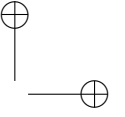
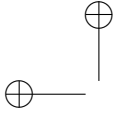
The redistribution of dopant in the base material is obtained from the mass transfer equation.

$$\frac{\partial c_m}{\partial t} + (\mathbf{u} \cdot \nabla) c_l = \nabla \cdot \left(\frac{1}{Pe} \nabla c_m \right) \quad (2.26)$$

Here, c_m is the net composition of the solid-liquid mixture, c_l is the composition of the liquid. $Pe = U'L/D$ is the Peclet number with D to be the molecular diffusivity of the dopant. In this equation, the diffusion coefficient D is taken as:

$$D = D_s(1 - \chi) + D_l\chi \quad (2.27)$$

where D_s and D_l denote the diffusion coefficients in solid and liquid, respectively.



CHAPTER 3

Modelling surfactant mass transfer in liquid metal system

3.1. Overview

Interfacial phenomena play a major role in nature as well as in material processes where more than one phase is involved. In metallurgical processes, the interfacial characteristics of liquid metal, molten slag and gas systems, represents a significant part of the metallurgical process and to a certain degree, it will control the quality of the product.

In the bulk of a liquid, molecules are subject to intermolecular forces that averaged over time are symmetrical and have no net effect. However, the molecules at the surface, for example liquid-gas, do not have other similar molecules on all sides of them. Due to the small attraction between the molecules in gas phase, the liquid molecules at the interface are mainly attracted inward to the bulk. Therefore, there is a net attractive force towards the bulk, which is balanced by the resistance of the liquid to compression. There may also be a small outward attraction caused by gas molecules. However, because the gas is much less dense than the liquid, this force is negligible. This complicated interplay of forces results in what we recognize as surface tension.

The interaction of a molecule at an interface involves a sequence of three reactions: adsorption, surface interaction and desorption. From historical point of view, the chemists studied equilibria of adsorption from the gaseous phase concerning the variations in composition of surfactant in relation to adsorption or segregation phenomena. The metallurgist was faced with the problem of redistribution of the impurities in the interface.

Any factor, which decreases the strength of the interaction at the surface, will lower the surface tension. Temperature is one of the factors that affect the surface tension. The other factors, i.e. surface active elements, or surfactants, are the larger class of molecules that have a significant importance for the surface tension. Generally, the existence of surfactant at the interface may lower the imbalance in the intermolecular forces and thus, reduces the surface tension. In liquid metals, the surface tension has been proved to depend considerably on the adsorption of surface-active elements such as sulfur, oxygen or nitrogen, etc. Belton (1976); Keene *et al.* (1982); Sahoo *et al.* (1988).

There are two main models for the surfactant molecule transport and adsorption. The *diffusion controlled* model, Figure 3.1, was first introduced by Ward and Tordai in 1946. A number of researchers Hansen (1960); Mysels (1982) have used this model

18 3. MODELLING SURFACTANT MASS TRANSFER

by assuming that the diffusion of the surfactant molecules in the bulk constitutes the limiting barrier to adsorption, and it is directly adsorbed to the interface once in the subsurface. The *mixed kinetic-diffusion* model offers a different scenario assuming there is a kinetic adsorption barrier that prevents the surfactant from adsorbing to the interface. In this model, the surfactant diffuses from the bulk to the subsurface layer by the same diffusion equation as in the bulk. However, once in the subsurface, the surfactant is not instantaneously adsorbed at the interface. Only those molecules that possess energy greater than a specified adsorption barrier, energy will be able to adsorb. Baret (1968); Stebe & Barthés-Biesel (1995); Chen & Stebe (1997). The mixed kinetic-diffusion model draws the great interest since almost practical applications of surfactant involve the use of surfactant mixture.

From the beginning of the last century, based on an empirical relation between the molality of the solution and the surface tension of the pure solvent, Szyszkowski indicated the effect of surface-active elements in liquid metals. After that, several studies Bernard & Lupis (1974); Belton (1976); Benard (1983) have attempted to describe the mechanism of the adsorption process of the surfactant at the liquid metals interface through general considerations or by theoretical treatments based on statistical thermodynamics. In 1976, Belton used a combination of the Gibbs and the Langmuir adsorption isotherms to develop a similar relation that described the surface tension of a liquid metal in the presence of a surface-active element. To demonstrate how the temperature coefficient of surface tension had changed with both temperature and composition of surface-active elements such as oxygen or sulfur, Sahoo *et al.* (1988) included the temperature dependence of the surface tension for the pure metal to Belton’s work. Up to today, many weld pool simulation models have been based on the research of Sahoo *et al.* (1988). The surfactant concentration has assumed to be constant at equilibrium during simulations with these models: Zacharia *et al.* (1989a), Ushio & Wu (1997), Winkler *et al.* (1998) and DebRoy (2001).

In the absence of motion, the surfactant adsorbed along the interface establishes an equilibrium surface concentration Γ_{eq} . However, temperature gradients of liquid metals is extremely high, which causes strong convection at the free interface of the liquid metal. With this convection, the molecules in the bulk and in the free surface are redistributed due to convection and diffusion. Figure 3.1 shows the fundamental processes involving the case of a binary liquid metal containing solvent and surfactant in a container. In this figure, the melt liquid is subdivided into three regions: the surface, the subsurface and the bulk. The surface is supposed to be a Langmuir monolayer, Adamson & Gast (1997), forming a layer that is only one molecule or atomic diameter in thickness. The subsurface layer is an important aspect of kinetic models that state these act as a barrier allowing reversible diffusion of surfactant into the bulk.

It has long been known that surface tension gradients in liquid metals have driven Marangoni convection and dominated the spatial distribution of liquid components, Shih & Stroud (1985). Especially in weld pools since the temperature gradient is very high, the Marangoni convection becomes very important. Hence, the effect of

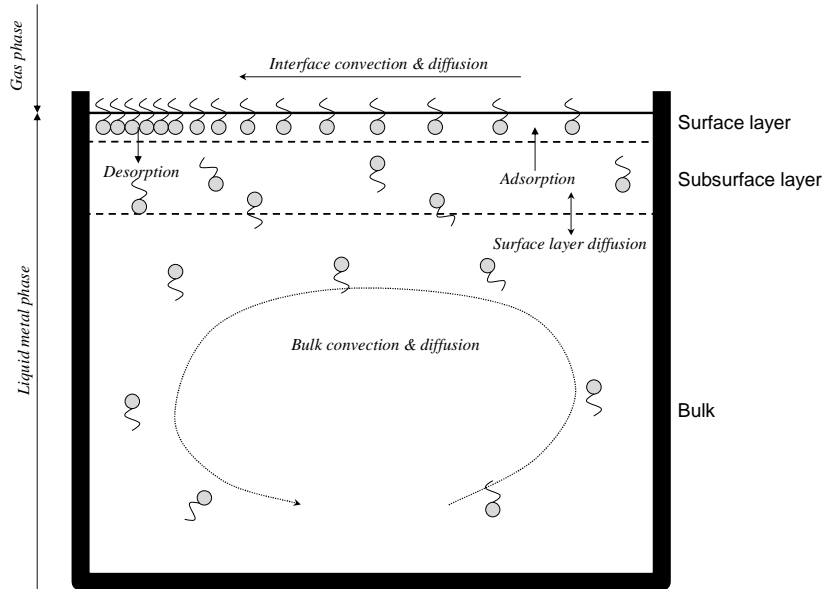


FIGURE 3.1. Fundamental processes of the transport and adsorption of surfactant to the interface.

convection to the surfactant cannot be neglected. Recently, several investigators Ginley & Radke (1988); Stebe & Barthés-Biesel (1995) studied the interaction between surfactant physicochemistry and fluid mechanics in a semi-infinite bubble progression model. They focused on the effect of the motion on the surface at the leading end of the bubble to the redistribution of the surfactant and introduced a steady non-equilibrium surface concentration transport equation. Winkler *et al.* (2000b) applied the physicochemical approach to the redistribution of surfactant at the surface and in the bulk for a time-dependent axisymmetric weld pool. With the inclusion of the redistribution of surfactant at the surface, the simulation results were claimed to adapt better to the experimental weld pool shapes.

3.2. Numerical model

In the model of the mixed diffusion-kinetic controlled adsorption, the rates of adsorption-desorption between the interface and the sublayer is entered to the equation of Γ as,

$$\frac{\partial \Gamma}{\partial t} + \nabla_s \cdot (\Gamma \mathbf{u}_s) = \frac{1}{Pe_s} \nabla_s^2 \Gamma + k_\beta C_s (\Gamma_\infty - \Gamma) - k_\alpha \Gamma \quad (3.1)$$

where, Γ is the surfactant content per unit area at the surface, ∇_s is a surface gradient operator, \mathbf{u}_s is the surface velocity, $Pe_s = U'L/D_s$ is the surface Péclet number which relates surface convection rates to surface diffusion rates, D_s . Γ_∞ is the upper bound on the surfactant concentration for monolayer adsorption. k_β and k_α are the kinetic

20 3. MODELLING SURFACTANT MASS TRANSFER

constants for adsorption and desorption, respectively. Those rates could be expressed in an Arrhenius type dependence, Ravera *et al.* (1993).

$$k_{\beta} = f_{\beta}(\bar{v}) \exp\left(-\frac{\varepsilon_{\beta}}{RT}\right) \quad (3.2)$$

$$k_{\alpha} = f_{\alpha}(\bar{v}) \exp\left(-\frac{\varepsilon_{\alpha}}{RT}\right) \quad (3.3)$$

where ε_{β} and ε_{α} are the energy barrier to adsorption and desorption. \bar{v} is the mean velocity of the surfactant molecules and RT is the product of the ideal gas constant and the absolute temperature.

The surfactant at the surface directly modifies the surface tension by the surfactant equation of state, $\gamma = f(\Gamma)$. For example the Frumkin equation of state as,

$$\gamma = \gamma_{eq} + RT\Gamma_{\infty} \ln\left(1 - \frac{\Gamma}{\Gamma_{\infty}}\right) \quad (3.4)$$

where γ_{eq} is the surface tension of pure melt at the melting point.

Belton (1976); Belton & Hunt Medalist (1993) applied the same combination of the Gibbs and Langmuir adsorption isotherm and pointed out that, for the ideal adsorption and the monolayer model, the value of the adsorption coefficient for a liquid metal might be related to the surface tension through the presence of a surface-active element a_i .

$$\gamma = \gamma_{eq} - RT\Gamma_{\infty} \ln(1 + K_{seg}a) \quad (3.5)$$

where the equilibrium constant for segregation K_{seg} is obtainable from (3.6), k_l is a constant related to the entropy of segregation and ΔH_0 is the standard heat of adsorption.

$$K_{seg} = k_l \exp\left(-\frac{\Delta H_0}{RT}\right) \quad (3.6)$$

At thermodynamical equilibrium, the surface tension equation of state - in which the constant coefficients (A , K_{seg}) were computed from experimental data - was rewritten by Sahoo *et al.* (1988) as:

$$\gamma = \gamma_{eq} - AdT - RT\Gamma_{\infty} \ln(1 + K_{seg}a) \quad (3.7)$$

where A is the negative of $d\gamma/dT$ for pure metal.

CHAPTER 4

Numerical methods

The Finite Element Method is a numerical analysis technique for obtaining approximate solutions to a wide variety of engineering problems. This is a useful and flexible method to approximate the solutions of partial differential equations with boundary conditions. In some problems, the regions of interest appear only in certain parts of the domain and the location of these is time dependent. To solve such problems, the mesh can be adapted to the regions of interest and make the computation more concentrated on the regions. In addition, this method is suitable for the automated code generation procedure.

In this chapter, an extended version of femLego, Amberg *et al.* (1999), is presented. The code is generated automatically in C/C++ and Fortran 77. This code runs on parallel computers by using the message passing protocol library (MPI).

4.1. Solving algorithm

Both the welding problem and the floating zone problem can be simulated by using the incompressible, time dependent Navier-Stokes equations. The melt is treated as an incompressible Boussinesq liquid in the welding pool as well as an incompressible Newtonian liquid in the floating zone.

$$\nabla \cdot \mathbf{u} = 0 \quad (4.1)$$

$$\frac{\partial \mathbf{u}}{\partial t} + (\mathbf{u} \cdot \nabla) \mathbf{u} = -\frac{1}{\rho} \nabla p + \nu \nabla^2 \mathbf{u} + \mathbf{S} \quad (4.2)$$

where, \mathbf{u} is the fluid velocity; p is the pressure, and \mathbf{S} is the source term, that included the Lorentz force, the natural convection, etc.

To solve the Navier-Stokes equations, the author applied a method that is modified from the projection method of by Guermond & Quartapelle (1998). We use the same element type, piecewise linear tetrahedral element, for all velocity, pressure and temperature variables. The elements could be refined or merged back to the original element size by using the adaptive finite element method. The restrictions imposed by Babuska-Brezzi condition were avoided by adding a pressure stabilization term, see Hansbo & Szepessy (1990). The pressure and velocity solutions are split using a fractional step algorithm. The discretised Poisson equation of the pressure is symmetric and positive definite, and is solved by using the well-known Conjugate-Gradient method for less computation time, especially in parallel computing. The convective terms in the momentum equation and thermal equation are calculated implicitly using the GMRES method. The streamline-diffusion method, Zienkiewicz & Taylor (2000),

22 4. NUMERICAL METHODS

has been added to those equations in order to enhance stability without loosing accuracy. To determine the overall stability of the numerical scheme, a Courant number is introduced,

$$Co = u_{max} \frac{dt}{dx} \quad (4.3)$$

where u_{max} is the maximum velocity in the x-direction in the domain and dx is the spatial step size. In the present semi-implicit treatment of convective terms, a practical value of the Courant number should not exceed a critical value of 2.5. Here, minimum grid space is 0.02 mm and maximum velocity can reach 1 ms^{-1} . Hence, the maximum time step that can be applied in this case, is $5 \times 10^{-5} \text{ s}$.

A fully implicit method has been adopted for the concentration equations. At each time step, the bulk concentration $C(x, y, z)$, and the surface concentration $\Gamma(x, y, z)$ are solved by using an iterative procedure. At a new time step, initial iterative fields are set to previous time step values ($\tilde{\Gamma}, \tilde{C}$), then the following iterative system is solved:

$$\frac{\tilde{\Gamma}^{n+1} - \Gamma^n}{\Delta t} + \nabla_s \cdot (\tilde{\Gamma}^{n+1} \mathbf{u}_s^n) = D_s \nabla_s^2 \tilde{\Gamma}^{n+1} + j_n \quad (4.4)$$

$$\frac{\tilde{C}^{n+1} - C^n}{\Delta t} + \nabla \cdot (\tilde{C}^{n+1} \mathbf{u}^n) = D_m \nabla^2 \tilde{C}^{n+1} \quad (4.5)$$

$$(4.6)$$

where i is the index of iteration level. Δt is the time step. Equations (4.5) and (4.6) are repeated until

$$\|\tilde{\Gamma}^{n+1} - \tilde{\Gamma}^n\| < \varepsilon \quad \text{and} \quad \|\tilde{C}^{n+1} - \tilde{C}^n\| < \varepsilon \quad (4.7)$$

During the presented calculations, we used $\varepsilon = 10^{-8}$ and the values at the new time step $n + 1$ of $\Gamma^{n+1} = \tilde{\Gamma}^{n+1}$ and $C^{n+1} = \tilde{C}^{n+1}$.

4.2. Parallel adaptive computation

A new parallel version of **femLego**, a finite-element tool for partial differential equations has been developed within the scope of this project. This tool is based on the automated code generation, Amberg *et al.* (1999). Parallelism is implemented using MPI and decomposes the problem spatially into an unstructured collection of blocks. Here, the ParMetis library, Karypis & Kumar (1998), is used for the mesh partitioning and adaptive repartitioning. Figure 4.1 shows an example of the mesh divided into four partitions that is used in the welding calculation. The algorithm yields excellent scaling on both shared memory and distributed memory architecture machines, with the latter yielding a performance improvement factor approximately linear with the numbers of processors used, Figure 4.2.

Figure 4.2 shows the speed up of the calculation on an IBM-SP2 machine and a PC-cluster at PDC, KTH. The speed-up is acceptable on both the IBM-SP2 and the PC-cluster. In this calculation, the welding pool is simulated on a fixed mesh. This mesh is partitioned and distributed to each processors at one in the initial time only.

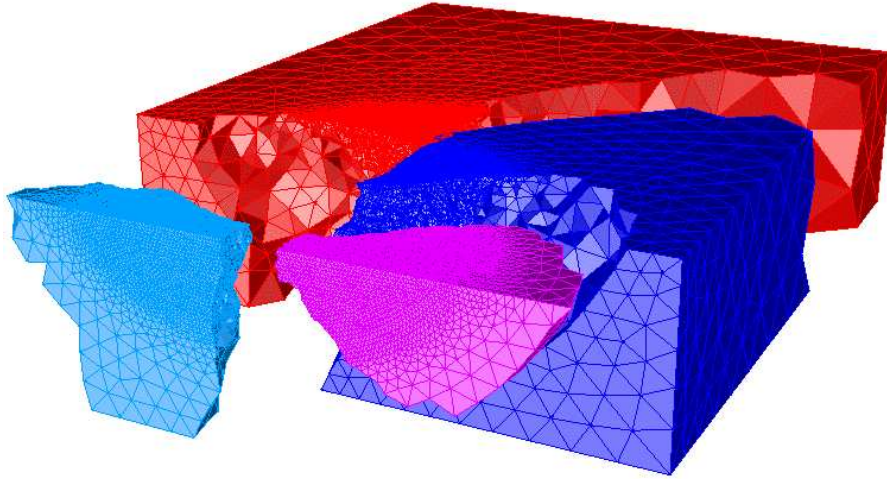


FIGURE 4.1. Example of mesh partitioning on 4 processors

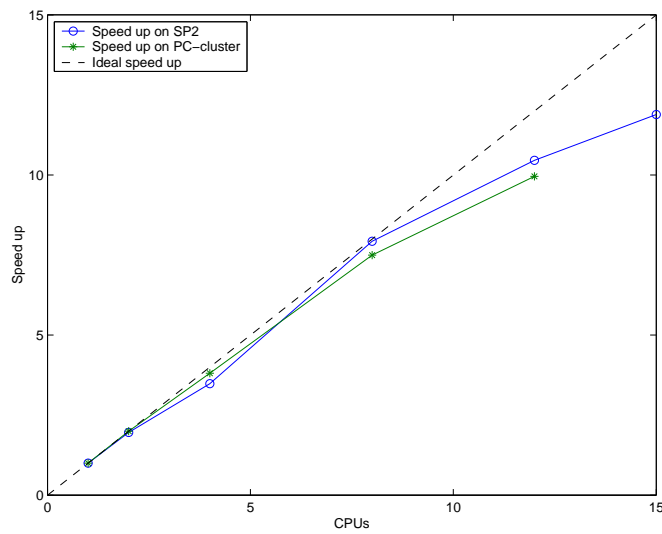


FIGURE 4.2. Performance of parallel computing. Mesh size: 125000 nodes and 680000 tetrahedra elements

The latest version of femLego with an adaptive mesh refinement and derefinement has been developed recently. The adaptivity is now done in parallel. The new scheme “level of node and face” was introduced in order to reduce the interprocessor communication on the adaptive mesh refinement and derefinement. With the new

24 4. NUMERICAL METHODS

scheme, the information needed for the derefinement is kept locally and the history tree information is not needed.

This tool used Rivara’s longest edge bisection scheme in 2D refinement and derefinement, Rivara (1989), and Arnold’s scheme for 3D, Arnold *et al.* (2000). The adaptivity in both schemes is done in parallel and the level of node-edge or node-face scheme are introduced in order to reduce cost of the information exchange between processors.

The new tool is now used to simulate the floating zone and the fusion welding, where the solid interface is moving. The performance of parallel adaptive mesh refinement and derefinement are shown on Figure 4.3. Curve (A) shows the speed up of the parallel code on different number of processors. This data based on the total computational time needed to compute for a short time interval of the real weld process, $t = 1.5s$ to $1.52s$. During this period, the mesh size increased from 770,000 elements and 141,400 nodes to 792,000 elements and 145,642 nodes. Curve (B) represents the speed up of the computation at the period where the weld pool is fully developed, at t around 3.5s. The mesh size now is nearly constant at 1,100,000 elements and 207,000 nodes.

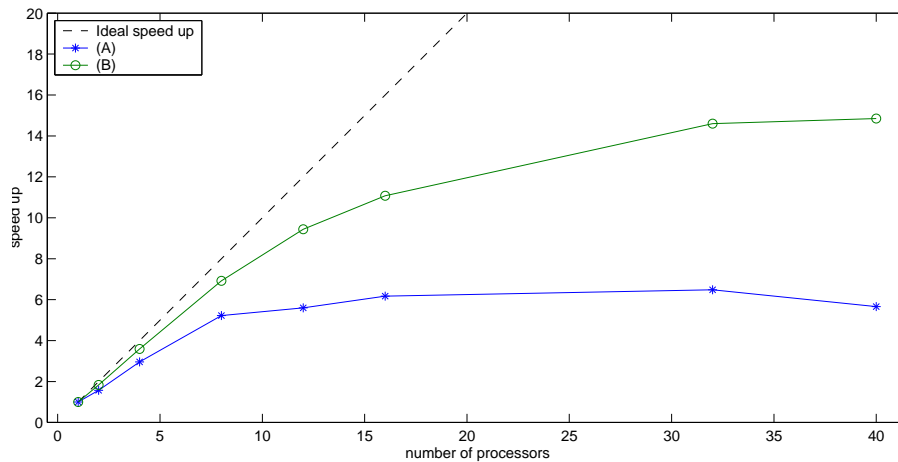


FIGURE 4.3. Performance of parallel computing for finite element adaptive code.

At the fully developed stage, the speedup curve shows very good performance. It is nearly comparable with the previous result for the parallel finite element without adaptivity, Figure 4.2. Meanwhile, during the development stage, when the solidification interface was still expanding, the speedup is very good up to 8 processors, and shows a poor performance with the higher number of processors. Altogether, this code shows good performance for the simulation of welding.

4.3. Automated code generation

The original femLego tool, Amberg *et al.* (1999), has been modified to be able to produce a code that can run on parallel computers. As in the previous version, the partial differential equations, the boundary conditions and initial conditions as well as the method of solving each equation can all be specified in a Maple worksheet. A set of C programs have been produced as a linkage between the MPI library and the Fortran core code. The Fortran core code takes responsibility for assembling stiffness matrices and right hand sides. The adaptive refining / derefining of the mesh is done in a separate ‘black box’, which takes as input of the last computed result. Using an error estimate as defined in the Maple worksheet, regions that are to be refined or coarsened are determined. A diagram of the femLego parallel version is shown in Figure 4.4.

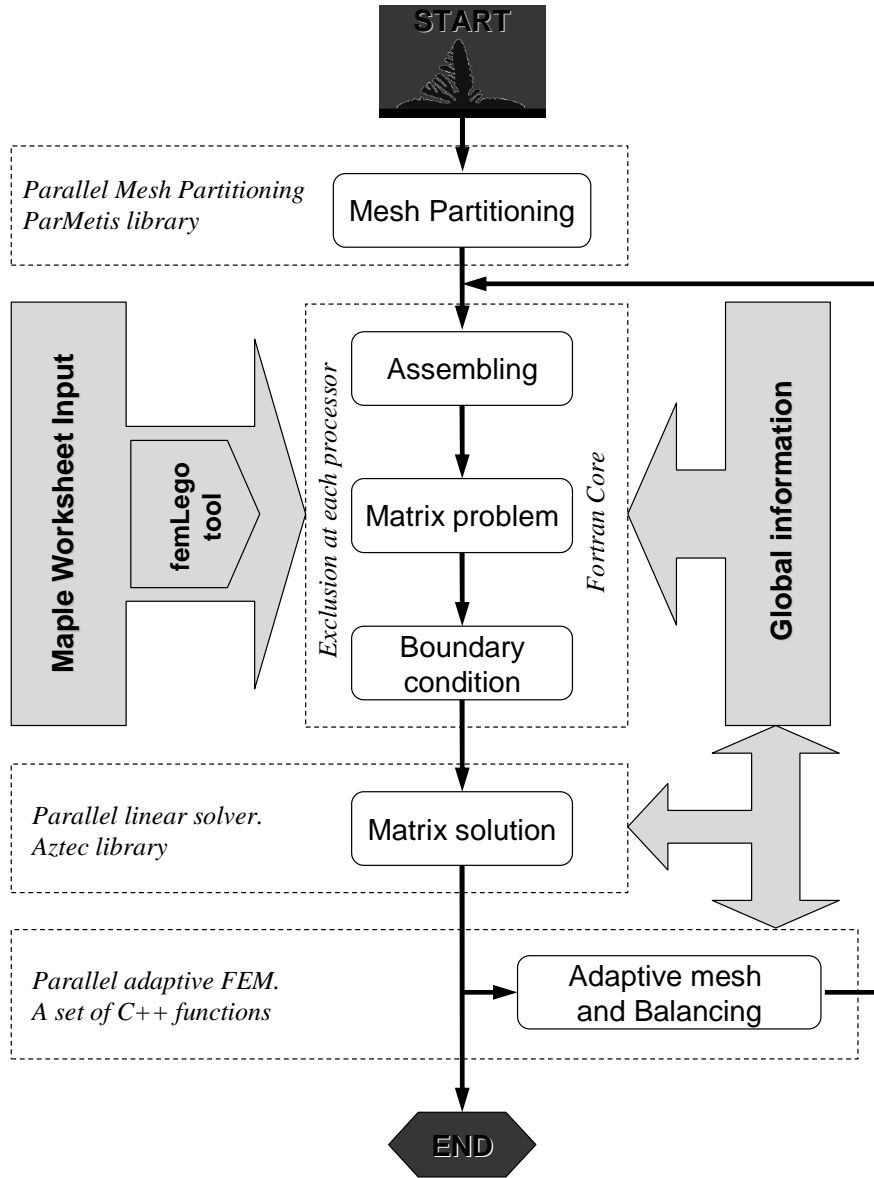


FIGURE 4.4. Flow chart of femLego parallel version

CHAPTER 5

Summary of papers

In this chapter, the papers are reviewed briefly. The summary is mainly used to illustrate the coupling between the papers, even if some of them are of different character.

Paper 1. Modelling of time-dependent 3D weld pool flow due to a moving arc.

This paper is an extension from the previous paper of Winkler *et al.* (1998). The author of the thesis has strengthened the femLego tool so that it is able to run in parallel. It is now capable of solving time-consuming problems e.g. 3D welding pool simulation. The authors also introduced a new comprehensive numerical model of the time-dependent weld pool flow in GTA welding, with a moving heat source. This model included heat transfer, radiation, evaporation, electromagnetic forces and Marangoni stress in the free surface boundary. With this 3D, fully time-dependent model, the truly chaotic, time-dependent melt flow was obtained.

The time-dependent properties of flow velocities and temperature of numerical results are examined. It shows that the temperature fields are strongly affected by convection at the weld pool surfaces. The fluid flow in the weld pool is highly complex and it influences the weld pool's depth and width. Moreover, the velocity field at the surface of the specimen determines the streamlines defining the traveling paths of inclusions such as slag particles.

Paper 2. Modelling of time-dependent 3D weld pool flow.

In this paper, the author has deepened his study of the time-dependent problem in different materials. The presented modelling results are the time-dependent weld pool flow and the temperature in gas tungsten arc welding (GTA) of the different types of stainless steels. It shows that the temperature fields are strongly affected by the convection at the weld pool's surfaces. With the stainless steel type 304 (low sulfur content of 0.0005 wt % and high sulfur content of 0.0139 wt %), the actual chaotic time-dependent melt flow is obtained with a fully time-dependent model. In those cases, the fluid flow in the weld pool is highly complex and influences the weld pool's depth and width. For the 645 SMO steel, which has an extremely low sulfur content and low thermal conductivity, the chaotic fluid flows did not appear. The calculated geometry of the weld fusion zone and heat affected zone were in good agreement with the experimental results, both with and without chaotic fluid flows.

28 5. SUMMARY OF PAPERS

Paper 3. Experimental and Numerical study of the influence of sulfur redistribution in welding of SAF-2507 stainless steel.

A physicochemical model was included to the previous model to allow redistribution of surfactant molecules at the surface of the weld pool as well as in the bulk liquid. Thus, instead of the equilibrium value for the surfactant content in the weld pool, the surfactant concentration could vary in the liquid pool and at the surface of the weld pool. The redistribution of surfactants was modeled by a mass transfer equation for the surfactant concentration. The numerical results were compared with experimental results for the stainless steel SAF-2507.

Paper 4. Modelling of the adsorption kinetics and the convection of surfactants in GTA welding.

This paper is an extension of paper 3. The surfactant binary system that was studied in the previous paper is now expanded to a ternary system. The model used in this paper is developed on the basis of the Langmuir adsorption isotherm. The Langmuir equilibrium adsorption ratio was founded on the experimental coefficient of Sahoo *et al.* (1988).

Paper 5. Three-dimensional time-dependent modelling of radial segregation due to weak convection.

A comprehensive three-dimensional, time-dependent model of heat, momentum and solute transfer during solidification is carried out to illustrate the influence of weak convection, caused by surface tension forces, on radial dopant segregation occurring in crystal growth under micro-gravity conditions. The author of the thesis has developed a 3D adaptive finite element method, which was used in order to simulate the motion and deformation of the solidification interface. The geometry studied is a Bridgman configuration with a partly coated surface. The small slots in the coating gave a free surface in a controlled way, and were varied in order to alter the Marangoni flow.

A comparison is made between the numerical results and the experimental results in this study. Good agreement has been observed for the effective distribution coefficient k_{eff} and for the radial segregation $\Delta c'$. The radial dopant segregation is strongly affected by weak convection.

Paper 6. Problem Solving Environment for Parallel Adaptive Computation.

This paper presents in detail the computing environment that has been used to generate codes for papers 1 to 6. A new scheme for minimization of the communication time in the parallel adaptive finite element method, node level and face level, is introduced. Together with the co-authors's works, this papers shows the efficiency of using parallel computing on the simulation of heat and mass transfer, material science and free boundary problems.

CHAPTER 6

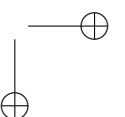
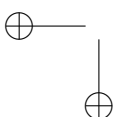
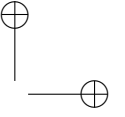
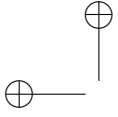
Conclusions and outlook

The long term goal of the work presented in this thesis concern the modelling of melt convection on fusion welding and floating zone crystal growth. The physical properties were studied and included as the fluid flows, heat transport phenomena on a three dimensional welding pool with a heat source moving. The model of floating zone has been adapted to account for the solidification interface moving and deformed by convection. The surface tension phenomena of liquid metal also consumed a lot of time during the work on this thesis. The effect of surfactants as sulfur, oxygen, etc., onto the surface tension of melt were studied. An included physicochemical approach allowed the surfactant concentration at the surface and in the bulk to depart from its thermodynamical equilibrium. The distribution of the surfactant was also found to be affected by the convection.

A very good agreement between the numerical simulation and the experiment of GTA welding was observed. The numerical simulation shows very detailed results of the fluid flow inside the welding pool. They were much more complex than that observed in previous 2D or quasi-steady 3D modelling results. The oscillation of melt flows occurred in the welding pool of the Type 304 stainless steel, where the sulfur content is high.

The finite element method with adaptive mesh has been successfully applied in parallel computers. It helped to capture the moving solidification interface in the numerical simulation of the floating zone. The radial segregation was obtained in the solidified material and a clear quantitative relation between the free surface area and the radial segregation was revealed. The dopant concentration results show a slight shift of the maximal concentration in the radial profiles. The experiments show a stronger effect, but there can be many reasons for the experimental scatter, e.g. uncompletely free surfaces over the slots.

With the new version of the femLego tool improved in the scope of this thesis, femLego now can be used to solve huge problems which are too time-consuming in serial computing. The powerfulness of the femLego tool has been demonstrated in the simulation of gas tungsten arc welding and the melt growth of semiconductor material using the floating zone technique.



Acknowledgment

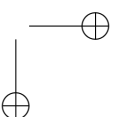
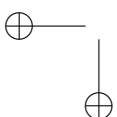
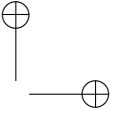
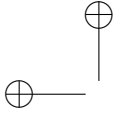
I would like to express my heartfelt gratitudes to my supervisor, Prof. Gustav Amberg for precious guiding, advise, inspiration, and constant support through my study. He also taught me many other valuable things in life and paid incredible patience.

I am also very thankful for Dr. Erik Aurell, my first supervisor in KTH, and Prof. Nam Dinh, the ones who led me to scientific computing and gave great efforts to help me set the very first steps in this very abundant world.

I also express my sincere thanks to the entire staffs, colleagues and friends at Department of Mechanics, Royal Institute of Technology, for providing an excellent study environment, especially Irina Singer-Loginova, Junichiro Shiomi, Per J. Olsson, Olle Törnblom, Walter Villanueva and Johan Gullman-Strand for collaboration, wonderful discussions as well as joyful sailing and fishing during the course.

Many thanks go to Parallel and Scientific Computing Institute (PSCI) and AvestaPolarit Stainless company and Sandvik Stainless company for financial supports and experimental experiences providing.

My deepest thank is conveyed to my wife Le Thanh Nga, my little son Do Quang Anh and my family and all friends for their endless love, inspiration, encouragement and supports in every aspects of my life.



Bibliography

- ADAMSON, A. & GAST, A. 1997 *Physical Chemistry of Surfaces*. John Wiley & Sons.
- ALEXANDER, J., QUAZZINI, J. & ROSENBERGER, F. 1989 *J. Crystal Growth* **97**, 285.
- AMBERG, G. 1991 Computation of macrosegregation in an iron-carbon cast. *Int. J. Heat Mass Transfer* **34** (1), 17–227.
- AMBERG, G., TÖNHARDT, R. & WINKLER, C. 1999 Finite element simulations using symbolic computing. *Mathematics and Computers in Simulation* **49**, 149–165.
- ARNOLD, D., MUKHERJEE, A. & POULY, L. 2000 Locally adapted tetrahedral meshes using bisection. *SIAM J. Sci. Comput.* **22** (3), 431.
- ATTHEY, D. 1980 A mathematical model for fluid flow in a weld pool at high currents. *J. Fluid Mech.* **98**, 787–801.
- BARET, J. 1968 Kinetics of adsorption from a solution. role of the diffusion and of the adsorption-desorption antagonism. *J. Phys. Chem.* **72** (8), 2755.
- BELTON, G. 1976 *Metall. Trans. B* **7B**, 35.
- BELTON, G. & HUNT MEDALIST, R. 1993 *Metall. Trans. B* **24B**, 241.
- BENARD, J. 1983 *Adsorption on metal surfaces*. Elsevier Scientific Pub. Co.
- BERNARD, G. & LUPIS, C. 1974 Statistical thermodynamics model of the adsorption of a surface active species on metals. *Surf. Sci.* **42** (1), 61.
- CARLBERG, T. 2004 Weak convection influencing radial segregation. In *Int. Symp. on Physical Sciences in Space*. Submitted.
- CHAKRABORTY, N., CHAKRABORTY, S. & DUTTA, P. 2004 Three-dimensional Modelling of turbulent weld pool convection in gta processes. *Numer. Heat Tr. A* **45**, 391.
- CHANG, C. & BROWN, R. 1983 Radial segregation induced by natural convection and melt/solid interface shape in vertical bridgman growth. *J. Crystal Growth* **63**, 343–364.
- CHEN, J. & STEBE, K. 1997 *J. Fluid Mech.* **340**, 35.
- CHOO, R. & SZEKELY, J. 1992 On the calculation of the free-surface temperature of gas-tungsten-arc weld pool. *Metall. Trans. B* **23B** (6), 371–384.
- CHOO, R. & SZEKELY, J. 1994 The possible role of turbulence in gta weld pool behavior. *Weld J.* **73** (2), 25s–31s.
- DEBROY, T. 2001 Mathematical Modelling of fluid flow and heat transfer in fusion welding. *Math. Modelling of Weld Phenomena* **5**, 1.
- EAGER, T. & TSAI, N. 1983 Temperature fields produced by traveling distributed heat sources. *Weld J.* **62** (12), S346.
- EHLEN, G., LUDWIG, A. & SAHM, P. 2001 Influent of welding power and welding duration on

34 BIBLIOGRAPHY

- the shape of the weld pool: Transient effect. *Mathematical Modelling of Weld Phenomena* **6**, 163–193.
- GINLEY, G. & RADKE, G. 1988 *ACS Symposium Series* **396**, 480.
- GUERMOND, J. & QUARTAPELLE, L. 1998 On stability and convergence of projection methods based on pressure poisson equation. *Int. J. Numer. Meth. Fluids*. **26**, 1039–1053.
- HANSBO, P. & SZEPESSY, A. 1990 A velocity pressure streamline diffusion finite-element method for the incompressible navier-stokes equations. *Comp. Meth. Appl. Mech.* **84** (2), 175–192.
- HANSEN, R. 1960 The theory of diffusion controlled absorption kinetics with accompanying evaporation. *J. Phys. Chem.* **64** (5), 637.
- HONG, K., WECKMAN, D., STRONG, A. & ZHENG, W. 2002 Modelling turbulent thermofluid flow in stationary gas tungsten arc weld pools. *Sci. Technol. Weld. Joi.* **7** (3), 125–136.
- JÖNSSON, B. & ÅGREN, J. 1986 Thermodynamic assesment of sb-sn system. *Mat. Sci. Techn.* **2** (9), 913.
- KARYPIS, G. & KUMAR, V. 1998 A fast and high quality multilevel scheme for partitioning irregular graphs. *SIAM J. Scientific and Statistical Computing* **20**, 359–392.
- KEENE, B., MILLS, K., BRYANT, J. & HONDROS, E. 1982 *Can. Metall. Quart.* **21** (4), 393.
- KHAN, P. & DEBROY, T. 1984 Alloying element evaporation and weld pool temperature during laser welding of aisi 202 stainless steel. *Metall. Trans. B* **15B**, 641.
- KIM, C. 1975 Thermophysical properties of stainless steels. *Tech. Rep.*. Argonne National Laboratory.
- KOU, S. 2002 *Welding Metallurgy*, 2nd edn. New York: John Wiley and Sons.
- KOU, S. & LE, Y. 1983 Three-dimensional heat flow and solidification during the autogenous gta welding of aluminum plates. *Metall. Trans. A* **14A**, 2245–2253.
- KOU, S. & SUN, D. 1985 Fluid flow and weld penetration in stationary arc welds. *Metall. Trans. A* **16A** (2), 203–213.
- LAN, C. 1996 Effect of axisymmetric magnetic fields on radial dopant segregation of floating-zone silicon growth in a mirror furnace. *J. Crystal Growth* **169** (2), 269.
- LAN, C. & YEH, B. 2004 Three-dimensional simulation of heat flow, segregation, and zone shape in floating-zone silicon growth under axial and transversal magnetic fields. *J. Crystal Growth* **262** (1-4), 59.
- LEVENSTAM, M., AMBERG, G., TILLBERG, E. & CARLBERG, T. 1990 Weak flow in a floating zone configuration as a source of radial segregation. *J. Crystal Growth* **104** (3), 641–652.
- LIE, K. & WALKER, J.S AMD RIAHI, D. 1990 Free surface shape and ac electric current distribution for float zone silicon growth with a radio frequency induction coil. *J. Crystal Growth* **100** (3), 450.
- MÜHLBAUER, A., MUIZNIEKS, A., RAMING, G., RIEMANN, H. & LÜDGE, A. 1999 Numerical modelling of the microscopic inhomogeneities during fz silicon growth. *J. Crystal Growth* **198-199** (1), 107.
- MÜHLBAUER, A., MUIZNIEKS, A., VIRBULIS, A., LÜDGE, A. & RIEMANN, H. 1995 Interface shape, heat transfer and fluid flow in the floating zone growth of large silicon crystals with the needle-eye technique. *J. Crystal Growth* **151** (1-2), 66.
- MÜLLER, G. 1998 Melt growth of semiconductors. *Materials Sciences Forum* **276-277**, 87–108.
- MUNDRA, K., BLACKBURN, J. & DEBROY, T. 1997 Absorption and transport of hydrogen during gma welding of low alloy steel. *Sci. Technol. Weld. Joi.* **2** (4), 174–184.

- MUNDRA, K., DEBROY, T. & KELKAR, K. 1996 Numerical prediction of fluid flow and heat transfer in welding with a moving heat source. *Numer. Heat Tr. A* **29** (2), 115–129.
- MYSELS, K. 1982 Diffusion-controlled adsorption kinetics. general solution and some applications. *J. Phys. Chem.* **86** (23), 4648.
- NIKITIN, S., POLEZHAYEV, V. & FEDYUSHKIN, A. 1981 *J. Crystal Growth* **52**, 471.
- OREPER, G., EAGAR, G. & SZEKELY, J. 1983 1983. *Weld J.* **62** (11), 307s–312s.
- OREPER, G. & SZEKELY, J. 1984 1984. *J. Fluid Mech.* **147**, 53–79.
- PALMER, T. & DEBROY, T. 2000 Numerical Modelling of enhanced nitrogen dissolution during gtaw. *Metall. Mater. Trans. B* **31B**, 1371–1385.
- PFANN, G. 1952 Principles of zone-melting. *Trans. of the American Inst. of Metals* **194**, 747–753.
- POLEZHAYEV, V. & NIKITIN, S. 1989 p. 237. Oxford.
- RATNIEKS, G., MUIZNIEKS, A., MÜHLBAUER, A. & RAMING, G. 2001 Numerical 3d study of fz growth: dependence on growth parameters and melt instability. *J. Crystal Growth* **230** (1-2), 48.
- RAVERA, F., LIGGIERI, L. & STEINCHEN, A. 1993 Sorption kinetics considered as a renormalized diffusion process. *J. Colloids and Interface Sci.* **156**, 109.
- RIVARA, M. 1989 Selective refinement/derefinement algorithms for sequences of nested triangulations. *Int. J. Numer. Meth. Eng.* **28**, 2889.
- ROSENTHAL, T. 1941 Mathematical theory of heat distribution during welding and cutting. *Weld J.* **20** (5), S220.
- ROSENTHAL, T. 1946 The theory of moving sources of heat and its application to metal treatments. *Transactions of the ASME* **68**, 849.
- SAHOO, P., DEBROY, T. & MCNALLAN, M. 1988 *Metall. Trans. B* **19B**, 483.
- SHIH, W. & STROUD, D. 1985 Theory of the surface tension of liquid metal alloys. *Phys. Rev. B* **32** (2), 804.
- STEBE, K. & BARTHÉS-BIESEL, D. 1995 *J. Fluid Mech.* **286**, 25.
- USHIO, M. & WU, C. 1997 Mathematical Modelling of three-dimensional heat and fluid flow in a moving gas metal arc weld pool. *Metall. Mater. Trans. B* **28B**, 509.
- WINKLER, C., AMBERG, G. & CARLBERG, T. 2000a Radial segregation due to weak convection in a floating zone. *J. Crystal Growth* **210**, 573–586.
- WINKLER, C., AMBERG, G., INOUE, H. & KOSEKI, T. 1998 A numerical and experimental investigation of qualitatively different weld pool shapes. *Mathematical Modelling of Weld Phenomena 4* pp. 37–69.
- WINKLER, C., AMBERG, G., INOUE, H., KOSEKI, T. & FUJI, M. 2000b The effect of surfactant redistribution on the weld pool shape during gta-welding. *Sci. Tech. Weld. & Join.* **5**, 1.
- YANG, Z. & DEBROY, T. 1999 Modelling macro-and microstructures of gas-metal-arc welded hsla-100 steel. *Metall. Mater. Trans. B* **30** (3), 483–493.
- YANG, Z., ELMER, J., WONG, J. & DEBROY, T. 2000 Evolution of titanium arc weldment macro and microstructures - Modelling and real time mapping of phases. *Weld J.* **79** (4), 97S–112S.
- ZACHARIA, T., DAVID, S., VITEK, J. & DEBROY, T. 1989a Weld pool development during gta and laser-beam welding of type-304, part i - theoretical analysis. *Weld J.* **68** (12), S499.
- ZACHARIA, T., DAVID, S., VITEK, J. & DEBROY, T. 1989b Weld pool development during gta and laser-beam welding of type-304, part ii - experimental correlation. *Weld J.* **68** (12), S510.

36 BIBLIOGRAPHY

- ZACHARIA, T., DAVID, S., VITEK, J. & KRAUS, H. 1991 Computational Modelling of stationary gas-tungsten-arc weld pool and comparison to stainless steel 304 experimental results. *Metall. Mater. Trans. B* **22**, 243.
- ZACHARIA, T. & ERASLAN, A. 1988*a* Modelling of autogenous welding. *Weld J.* **67** (3), S53.
- ZACHARIA, T. & ERASLAN, A. 1988*b* Modelling of non-autogenous welding. *Weld J.* **67** (1), S18.
- ZHAO, H. & DEBROY, T. 2001 Weld metal composition change during conduction mode laser welding of aluminum alloy 5182. *Metall. Mater. Trans. B* **32** (1), 163–172.
- ZIENKIEWICZ, O. & TAYLOR, R. 2000 *The Finite Element Method*, , vol. 3. Oxford: Butterworth Heinemann, cop.